

High-Pressure Elasticity and Auxetic Property of α -Cristobalite

Hajime Kimizuka^{1,2,*}, Shigenobu Ogata^{1,3} and Yoji Shibutani^{1,3}

¹Department of Mechanical Engineering, Graduate School of Engineering, Osaka University, Suita 565-0871, Japan

²Engineering Technology Division, The Japan Research Institute, Limited, Tokyo 102-0082, Japan

³Center for Atomic and Molecular Technologies, Graduate School of Engineering, Osaka University, Suita 565-0871, Japan

The structural variations with pressure in α -cristobalite, a low-density polymorph of SiO₂, have been studied through first-principles calculations using the projector-augmented-wave (PAW) method, with particular emphasis on its elastic and auxetic properties. We provide theoretical *ab initio* results for the volume compressibility and a complete set of independent elastic constants of cristobalite under hydrostatic pressures up to 10–15 GPa. Our calculated structural and elastic properties under pressure are in good agreement with the experimental data. In addition, the corresponding results of the molecular-dynamics simulations with the interatomic potential are also presented for comparison. The dominant mechanism of compression is the reduction of the Si–O–Si angles within the α -cristobalite structure, whereas the SiO₄ tetrahedron undergoes only a slight distortion. α -Cristobalite is more compressible than other SiO₂ polymorphs as shown by their volume compressibilities, because of its characteristic framework structure similar to re-entrant honeycombs. With increasing pressure, the rotational motions of the rigid SiO₄ tetrahedra play an important role in the compressive behavior of cristobalite. The present simulations confirm that the system undergoes transformation from auxetic to non-auxetic under hydrostatic pressure of ca. 2 GPa, while retaining strong elastic anisotropy.

(Received December 21, 2004; Accepted February 17, 2005; Published June 15, 2005)

Keywords: negative Poisson's ratio, auxetic materials, elastic constant, Birch-Murnaghan equation of state, density functional theory, molecular dynamics

1. Introduction

Properties and behavior of silicon dioxide (SiO₂) at high pressures and/or temperatures are of great interest due to its wide ranging implications in fundamental physics, geophysics and material science. It is known that SiO₂ can exist in many different crystalline forms, such as quartz, cristobalite, tridymite, coesite, stishovite *etc.* These forms (except stishovite) are typically three-dimensional network structures built of corner-shared SiO₄ units. The phases of SiO₂ serve as model systems for studies of high-pressure structures, phase transitions and chemical bonding.

For the last decade, low-temperature (α) phase of cristobalite has received much attention due to its peculiar elastic properties related to the 'auxetic' behavior at the molecular level.^{1–4} The marked characteristic of the auxetic materials is to exhibit a negative Poisson's ratio, and thus they can undergo lateral contraction under longitudinal compression and also lateral expansion under longitudinal tension [Fig. 1(a)]. Auxetic materials are of interest because of the novel behavior they exhibit under deformation, and also because such materials have possibility for improving mechanical properties, such as enhanced shear moduli, indentation resistance and fracture toughness.^{5–7}

The main objective of the present paper is to provide results of the atomistic simulations that can be used to evaluate quantitatively the high-pressure elasticity of cristobalite, and to investigate the microscopic mechanism for its compressive behavior associated with the auxetic nature. An understanding of the microscopic deformation process of such crystal is essential for leading the research into the modeling, design and development of auxetic nanomaterials. Here we apply the first-principles calculations to compute the structural properties and a complete set of independent elastic constants of cristobalite, under purely hydrostatic pressure.

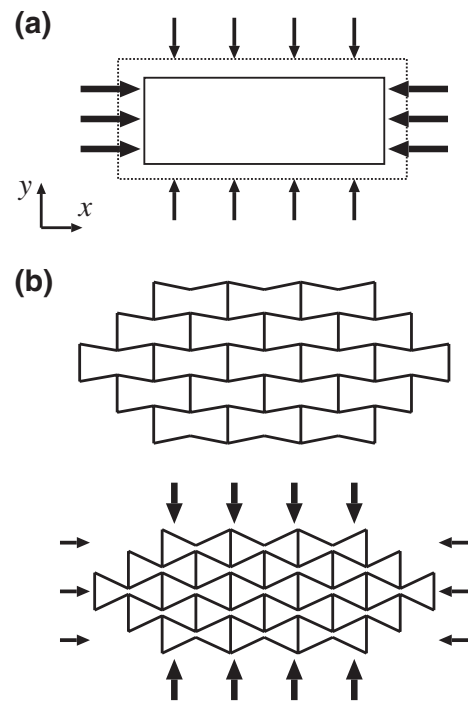


Fig. 1 Schematic diagram of negative Poisson's ratio (auxetic) deformation. (a) Auxetic behavior in which an initially undeformed material (dashed outline) undergoes longitudinal and lateral contraction (solid line) for a compressive load applied in the longitudinal (x) direction. (b) Re-entrant honeycomb undergoing deformation by hinging of the cell walls, leading to negative Poisson's ratio behavior.

Also, in this work we report the calculation of the pressure effects on elastic properties of cristobalite using equilibrium molecular dynamics (MD) method with the nonempirical pairwise interatomic potential by van Beest *et al.* (BKS).⁸ The BKS model has played important role over the last decade in numerous studies of silica and related materials. This work intends to establish a benchmark since few works

*Graduate Student, Osaka University.

have been reported on the quantitative accuracy of this model under pressure.

2. Computational Methods

2.1 First-principles calculations of α -cristobalite at high pressure

We have studied the compressive behavior of α -cristobalite using the Vienna Ab-initio Simulations Package (VASP).⁹⁾ The method implemented in this code involves computation of the self-consistent total energy, Hellmann–Feynman forces and stresses by solution of the Kohn–Sham equations based on density functional theory (DFT); and the subsequent relaxation of the electrons, atoms and unit cell. Total-energy minimization calculations under the applied pressure are performed using the projector-augmented-wave (PAW) method^{10,11)} within the local-density approximation (LDA).¹²⁾ For the exchange-correlation potential, the LDA functional given by Ceperley and Alder is employed,¹²⁾ and the parameterization of Perdew and Zunger¹³⁾ is used.

The simulations are started with a tetragonal primitive unit cell of α -cristobalite, containing four SiO_2 formula units, *i.e.* 12 atoms (space group $P4_12_12$).¹⁴⁾ A plane-wave basis set with a 1400 eV cutoff is adopted to expand the electronic wave functions at the special k points generated by a $4 \times 4 \times 4$ Monkhorst-Pack k mesh (6 irreducible k points).¹⁵⁾ We have checked the sensitivity of the elastic constants of α -cristobalite to an energy cutoff in the range 500–1400 eV, and a high-energy cutoff of 1400 eV is chosen in this case to obtain a satisfactory agreement with the experimental values. Here, the tetrahedron method with Blöchl corrections¹⁶⁾ is applied. The *ab initio* calculations of α -cristobalite are carried out by gradually increasing the pressure in 0.5–1.0 GPa increments for pressures up to 15 GPa. Forces on atoms and internal stress tensor are calculated, and atoms and cell parameters are allowed to relax using a conjugate gradient technique until their residual forces have converged to less than 0.1 eV/nm.

The crystal structure of α -cristobalite is tetragonal, *i.e.*, with two unit vectors of the same length ($a = b$), and thus its symmetry implies that there are six independent elastic constants for the phase. In order to calculate a complete set of independent elastic constants, affine strains are imposed on the unit cell in different directions, each corresponding to a certain elastic constant. However, it is known that the relaxation effects can be important for some materials, in particular, for auxetic crystals with internal degrees of freedom. Thus, the atomic coordinates are allowed to relax for each modification of the cell, leading to the general decrease of energy, and also the force on each atom is relaxed to less than 0.005–0.01 eV/nm.

2.2 Molecular dynamics simulations of α -cristobalite using an interatomic potential

Equilibrium molecular dynamics (MD) simulations of α -cristobalite have been performed starting from the α -phase at zero stress to the high-pressure phase continuously. We employ the effective pairwise interatomic potential proposed by van Beest *et al.* (BKS)⁸⁾ in the calculations reported here. It was derived from the cluster calculations of potential-

energy surfaces using the *ab initio* method for achieving high accuracy and transferability. The force-field parameters used in this work are given in Ref. 8). The Nosé–Hoover^{17,18)} and the Parrinello–Rahman¹⁹⁾ isothermal-isobaric thermostat is applied to realize the structures of the reference states at 300 K under nonzero external stress. In constructing the initial configurations of α -cristobalite, atoms are placed on experimentally determined positions.¹⁴⁾ The periodic simulation box for cristobalite is chosen to contain 48 ($= 4 \times 4 \times 3$) unit cells, so that the number of atoms in all MD calculations is 576, *i.e.* 192 silicon and 384 oxygen atoms. The hydrostatic pressure of the system is continuously raised up to the desired value ($P = 0, 5$ and 10 GPa) at a rate of 0.25 GPa/ps, after which the system is equilibrated over 80 ps. The integration time step in all MD simulations is 2 fs.

The adiabatic elastic constants at various pressures are calculated within the constant-volume and constant-energy ensemble, using the fluctuation formula for the internal stress tensor.²⁰⁾ The elastic constants under conditions of nonzero stress at a finite temperature are expressed by

$$V_0 h_{0ip}^{-1} h_{0jq}^{-1} h_{0kr}^{-1} h_{0ls}^{-1} C_{pqrs} = -\frac{4}{k_B T} \delta(M_{ij} M_{kl}) + 2Nk_B T \left(G_{li}^{-1} G_{jk}^{-1} + G_{ki}^{-1} G_{jl}^{-1} \right) + \left\langle \sum_{b>a} f(r_{ab}) s_{abi} s_{abj} s_{abk} s_{abl} \right\rangle_{av}, \quad (1)$$

where $\mathbf{M} = -(V/2)\mathbf{h}^{-1}\mathbf{P}\mathbf{h}'^{-1}$, \mathbf{P} denotes the internal stress tensor and V the volume containing the N particles, s_{abi} is a scaled coordinate related to the real coordinate by $x_{abi} = h_{ij}s_{abj}$, \mathbf{h}_0 is the value of the matrix for the case of zero stress, and \mathbf{h} is its value when the system is under the prescribed stress. The values of \mathbf{h}_0 and \mathbf{h} to be used in eq. (1) are obtained by carrying out appropriate *NTP* runs. T represents the temperature, k_B the Boltzmann constant, \mathbf{G} the metric tensor $\mathbf{G} = \mathbf{h}'\mathbf{h}$, and $f = r^{-2}(u'' - r^{-1}u')$ where the pair potential is denoted by $u(r)$. The fluctuation of a product of A and B is defined by $\delta(AB) = \langle AB \rangle_{av} - \langle A \rangle_{av} \langle B \rangle_{av}$ where the bracket represents the ensemble-average value. In order to check the validity of statistical sampling, the averages are separately taken every 80 ps during a 2.24-ns run for each pressure.

3. Results and Discussion

3.1 Structural variations with pressure

The lattice parameters of α -cristobalite at ambient pressure were evaluated using the DFT calculations and MD simulations with the BKS potential. The obtained values are $a_0 = 0.4928$ (0.49570) nm, $c_0 = 0.6835$ (0.68903) nm, $V_0 = 0.1660$ (0.16931) nm³ for the DFT calculations, and $a_0 = 0.4930$ [0.49709] nm, $c_0 = 0.6625$ [0.69278] nm, $V_0 = 0.1610$ [0.17118] nm³ for the BKS potential. Here, the numbers in round and square brackets are the experimental values¹⁴⁾ at 10 and 293 K, respectively. For both the methods, the calculated theoretical values are found to be slightly small (within 1–5%) but fairly close to those obtained from the neutron diffraction data.¹⁴⁾

With increasing pressure from 0 to 15 GPa, the unit-cell parameters decrease continuously with pressure and the

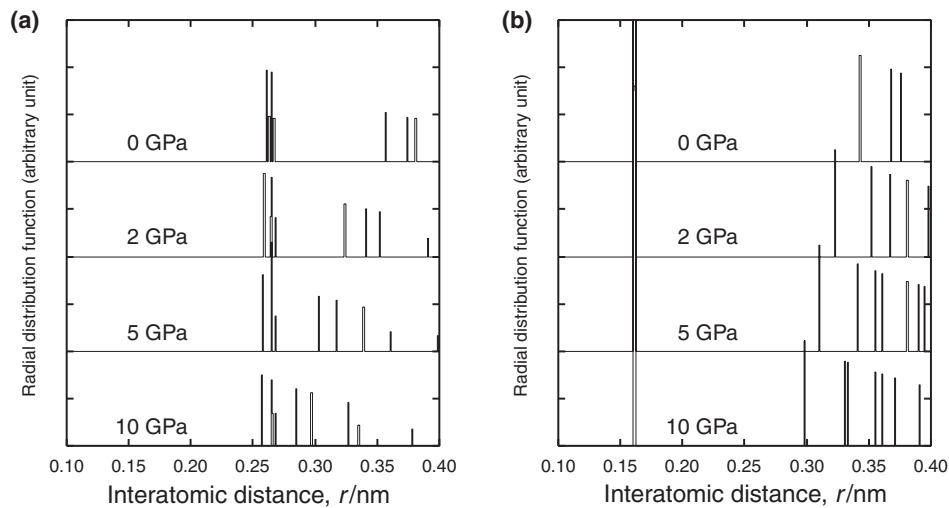


Fig. 2 Radial distribution functions for (a) O–O and (b) Si–O distances of α -cristobalite, from 0 to 10 GPa.

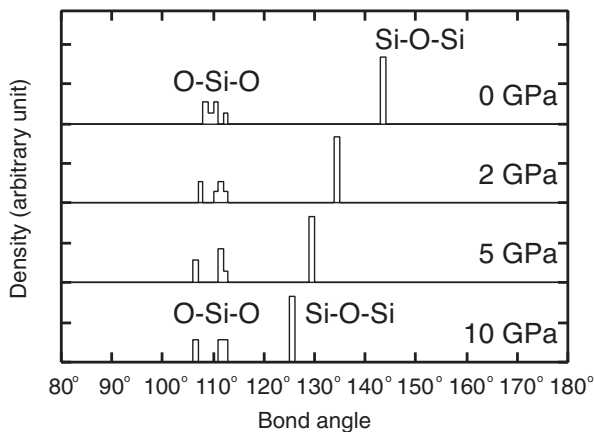


Fig. 3 Bond angle distribution functions for the O–Si–O and Si–O–Si angles in α -cristobalite, plotted against pressure.

system successively undergoes compressive deformation. Also, the tetragonal phase of cristobalite survives compression up to the applied pressure of 15 GPa, under the present symmetry conditions. Thus, the slightly distorted monoclinic cristobalite II structure as reported in Ref. 21) at $P = \text{ca. } 1.5 \text{ GPa}$ is not considered in our simulations.

To obtain information about the organization of neighboring atoms from the DFT results, the radial distribution functions for O–O and Si–O distances in cristobalite are calculated at various pressures, as presented in Fig. 2. Besides, the bond angle distribution functions for the O–Si–O and Si–O–Si angles are shown in Fig. 3. In Fig. 2 and Fig. 3, we confirm that the first-nearest Si–O and O–O distances, and the O–Si–O angles remain essentially unchanged up to the applied pressure of 10 GPa, and the rigid SiO_4 tetrahedral units in α -cristobalite structure are maintained during the compression. The only significant effect is in the Si–O–Si angle, which decreases from 143° at ambient pressure to 125° at 10 GPa, whereas the SiO_4 tetrahedra become slightly distorted (Fig. 3). In Fig. 2(a), the O–O distances beyond the nearest neighbors become much shorter

as the pressure increases, and we observe that the phase of α -cristobalite continuously evolves into the compressive phase up to 10 GPa, as shown in Fig. 4. Despite the large stiffness of tetrahedral units, the flexible framework structures readily undergo volumetric deformation through cooperative SiO_4 rotations, due to the weak interactions between SiO_4 tetrahedra. Structural studies at the lower pressures of $\sim 1.5 \text{ GPa}$ ^{1,22)} suggest that the pliant nature of the framework structure gives rise to the large compressibility and negative Poisson's ratio. In the present simulations, it is confirmed that the similar atomic-level compression mechanisms can be observed under hydrostatic pressures up to 10 GPa, within the α -cristobalite structure.

From the *ab initio* total-energy minimization calculations and the MD simulations with the BKS potential, the theoretical pressure-volume data were fit to the third-order Birch-Murnaghan equation of state (EOS) respectively, in the following form:

$$P = \frac{3}{2} K_0 (x^{\frac{7}{3}} - x^{\frac{5}{3}}) \left\{ 1 + \frac{3}{4} (K'_0 - 4) (x^{\frac{2}{3}} - 1) \right\}, \quad (2)$$

where K_0 and K'_0 denote the zero pressure bulk modulus and its pressure derivative, respectively, and $x = V_0/V$, where V_0 is the ambient unit cell volume. The fit yields $K_0 = 8.9(3) \text{ GPa}$ with $K'_0 = 10.5(5)$ for the DFT calculations, and $K_0 = 18.5(0)$ with $K'_0 = 9.4(0)$ for the BKS potential, respectively.

Figure 5 shows the volume compressibility curve obtained in the analysis, along with the x-ray diffraction data from Ref. 22) (solid triangle). In Fig. 5, the experimental data for cristobalite II²¹⁾ are also plotted as a guide (solid diamond). It is noteworthy that our theoretical data obtained from the DFT calculations are in good agreement with the experimental data, and also in accordance with the EOS for hydrostatic pressure. Here, the volume-compressibility data for the BKS potential are found to be overestimated from the experiment in the entire pressure range, and the system resists compression under pressure compared with the DFT system. Also, Fig. 5 indicates that α -cristobalite is more compressible than other SiO_2 polymorphs, such as α -quartz [$K_0 = 38.7$, $K'_0 =$

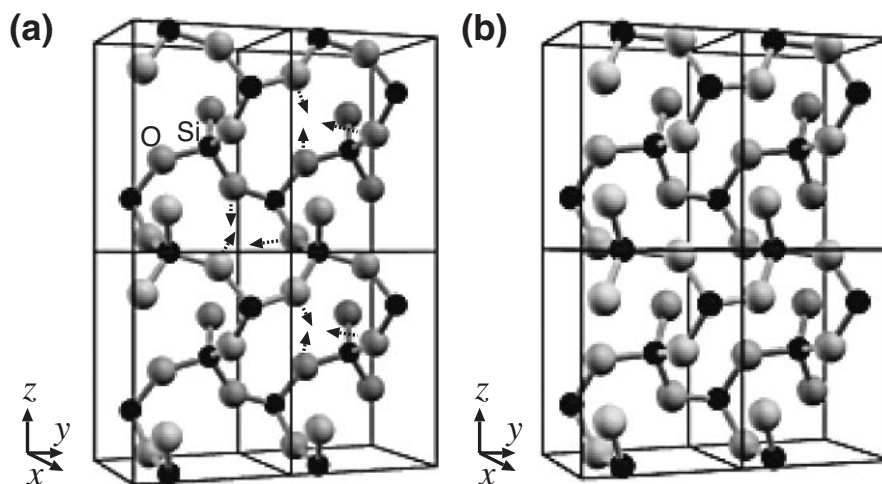


Fig. 4 Unit cells of α -cristobalite at (a) 0 GPa and (b) 10 GPa. The oxygen and silicon atoms are represented by the gray and black spheres, respectively.

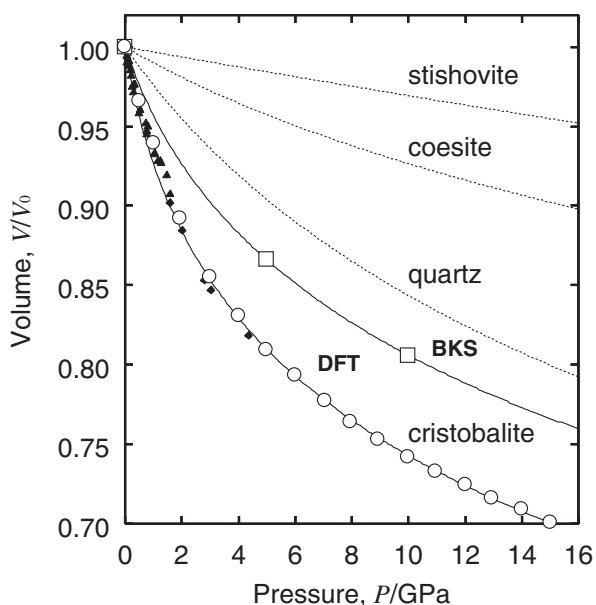


Fig. 5 Evolution with pressure of the unit-cell volume of α -cristobalite. The open circles and squares represent data from the DFT calculations and the MD calculations, respectively. The best fit Birch-Murnaghan equation of state [$K_0 = 8.9(3)$ GPa, $K'_0 = 10.5(5)$ for the DFT calculations, and $K_0 = 18.5(0)$ GPa, $K'_0 = 9.4(0)$ for the BKS potential] is represented as the solid curve. For comparison, the pressure-volume curves for quartz, coesite, and stishovite are shown as dashed lines. The x-ray diffraction data (solid symbols) are from Refs. 21, 22).

4.9 in Ref. 23)], coesite [$K_0 = 96$, $K'_0 = 8.4$ in Ref. 24)], and stishovite [$K_0 = 313$, $K'_0 = 2.8$ in Ref. 25)]. It is considered that this high compressibility of cristobalite is due to its auxetic nature at ambient pressure, and the cooperative motions of corner-linked SiO_4 tetrahedra play important role in the compressive behavior under hydrostatic pressure.

3.2 Pressure dependence of the elastic constants and Poisson's ratio

The adiabatic elastic stiffness constants (C_{ij}) of cristobalite were evaluated under pressures of 0–10 GPa using the DFT calculations and MD simulations with the BKS potential, respectively. The obtained C_{ij} values for the two methods are given in Table 1. We have included the experimental values¹⁾ for comparison, as well as the results of previous MD calculations^{3,27)} using the interatomic potential proposed by Tsuneyuki *et al.*²⁶⁾ (TTAM).

At ambient pressure, our calculated values are in good agreement with the experimental data, both for the DFT calculations and for the BKS potential. In particular for the DFT calculations, the shear components C_{44} and C_{66} are within 2–3% off the experimental values, while the bulk components C_{11} and C_{33} are off the experimental ones by around 9 and 16%, respectively. The deviation for two of C_{ij} 's, C_{12} and C_{13} , is rather high, around 40%. However, this high deviation can be understood from the fact that the two elastic constants have a low magnitude compared with the

Table 1 Calculated values for elastic constants, C_{ij} (in GPa), of α -cristobalite together with experimental values.

	$P = 0$ (GPa)			$P = 2$ (GPa)	$P = 5$ (GPa)		$P = 10$ (GPa)		
	Expt. ^a	DFT	BKS	TTAM ^b	DFT	BKS	DFT	BKS	
C_{11}	59.4	54.6	64.5	48.1	63.4	106.2	94.6	103.8	144.1
C_{33}	42.4	36.4	37.9	35.3	57.2	63.2	97.5	86.0	136.7
C_{44}	67.2	68.6	69.5	57.8	71.2	72.6	82.9	79.4	97.3
C_{66}	25.7	25.0	27.6	19.8	25.4	23.2	26.6	18.8	27.2
C_{12}	3.8	5.2	6.5	5.6	16.2	22.0	17.8	40.6	43.5
C_{13}	-4.4	-7.4	-0.7	-4.2	4.6	24.0	27.9	40.8	72.0

^aReference 1).

^bInteratomic potential by Tsuneyuki *et al.*²⁶⁾ [data from Ref. 3)].

Table 2 Isotropic bulk modulus (K in GPa), shear modulus (G in GPa), and Poisson's ratio (ν) of α -cristobalite.

	Expt. ^a	$P = 0$ (GPa)			$P = 2$ (GPa)		$P = 5$ (GPa)		$P = 10$ (GPa)	
		DFT	BKS	TTAM ^b	DFT	DFT	BKS	DFT	BKS	
K	16.37	13.4	18.8	13.6	25.9	45.0	48.1	59.6	88.6	
G	39.05	38.0	39.4	32.1	39.4	42.3	47.4	40.2	52.3	
ν	-0.163	-0.23	-0.12	-0.16	0.00	0.14	0.13	0.22	0.25	

^aReference 1).

^bInteratomic potential by Tsuneyuki *et al.*²⁶⁾ [data from Ref. 27].

other ones.

With increasing pressure up to 10 GPa, every component of the elastic constants except C_{66} tends to increase, while C_{66} is almost constant in this pressure range, for both the calculations. The C_{ij} values for the BKS potential, especially C_{11} , C_{33} , and C_{13} , are much larger than those obtained from the DFT calculations. This indicates that the model system of α -cristobalite interacting via the BKS potential is stiffer, and resists volumetric deformation under hydrostatic pressure. This corresponds to the results concerning the pressure-volume curves, as seen in Fig. 5. Through comparison with the DFT calculations, it is suggested that the compressive behavior and the high-pressure elasticity of α -cristobalite are not well described by the BKS model, whereas its force-field parameters are reasonably successful in describing the structural and elastic properties at ambient pressure.

The bulk modulus (K) and shear modulus (G) for an isotropic aggregate of cristobalite were evaluated from the C_{ij} 's by means of the Voigt-Reuss-Hill average. Table 2 shows K , G , and the Poisson's ratios (ν) of the single-phased aggregate of cristobalite at various pressures for the DFT calculations and the BKS potential, respectively. Here, ν values are derived by using the following formula for an isotropic solid:

$$\nu = \frac{3K - 2G}{2(3K + G)}. \quad (3)$$

The sign of a Poisson's ratio is determined by the relationship between K and G , as seen in eq. (3).

For the DFT calculations, the bulk modulus of α -cristobalite increases dramatically with hydrostatic pressure, whereas the shear modulus does not change and exhibits an almost constant value in the entire pressure range of 0–10 GPa. As a result, a negative value of the isotropic Poisson's ratio is observed only in the pressure region between ca. 0–2 GPa, and thus the system undergoes transformation from auxetic phase to non-auxetic phase at around 2 GPa, without the significant symmetry breaking during the compression. For the BKS potential, the bulk modulus exhibits a much larger value than those obtained from the DFT calculations, and the shear modulus increases gradually with pressure at 0–10 GPa. However, the similar pressure dependence and the change in the sign of a Poisson's ratio is also observed. In the lower pressure range of 0–2 GPa, α -cristobalite is susceptible to volumetric deformation, but is resistant to shear deformation against the stress, and thus a uniaxial compression leads to the volume contraction without change in shape. This fact coincides with the high compress-

sibility of α -cristobalite in the pressure range of 0–2 GPa (in Fig. 5), and the considerable increase of bulk modulus with pressure above ca. 2 GPa.

3.3 Anisotropy of Poisson's ratio

The directional property of a Poisson's ratio is investigated by the quotient of lateral to longitudinal strain, for all possible orientations of the coordinate system relative to the crystallographic axes. For a loading along the x_i direction, the Poisson's ratio ν_{ij} of a material is given by

$$\nu_{ij} = -\frac{S_{ji}}{S_{ii}} (i, j = 1, 2, 3), \quad (4)$$

where x_j is a transverse direction under consideration, and S_{ij} stands for the elastic compliance constants, the inverse of C_{ij} matrix. The variations in the ν_{12} , ν_{23} , and ν_{31} values for the α -cristobalite at various pressures are shown in Fig. 6.

In α -cristobalite at 0 GPa, the Poisson's ratio exhibits a marked anisotropy. Over all crystallographic directions its magnitude ranges from +0.07 to -0.59. However, its average exhibits a negative value (Table 2). The negative maximum value of $\nu_{23} = -0.59$ is obtained by rotating S_{ij} through approximately 42° from the b axis about the a axis. In α -cristobalite, this is the principal direction which shows a negative value of the Poisson's ratio. This negative value results from the typical framework structure of α -cristobalite which consists of uniform sixfold rings (Fig. 4). These rings have an inverted characteristic similar to re-entrant honeycombs, the typical model which induces a negative Poisson's ratio,^{28–30)} as shown in Fig. 1(b). At 10 GPa, the magnitude of the Poisson's ratio ranges from +0.48 to -0.22, and the rotation of S_{ij} about the a axis produces a maximum $\nu_{23} = -0.22$ at 44° from the b axis, while the isotropic value of the Poisson's ratio exhibits a positive value (Table 2). With increasing pressure, the range of a Poisson's ratio shifts gradually to a positive region, as seen in Fig. 6. However, its magnitude ranges from a negative to a positive values, and the structure retains high elastic anisotropy.

4. Conclusions

In conclusion, we have investigated the structural variations with pressure and the high-pressure elasticity of α -cristobalite, using both the *ab initio* DFT calculations with the PAW method and the MD simulations based on the BKS pairwise potential. Our DFT and MD approaches permit a description of the changes with pressure in the volume compressibility and the elastic properties of cristobalite, the

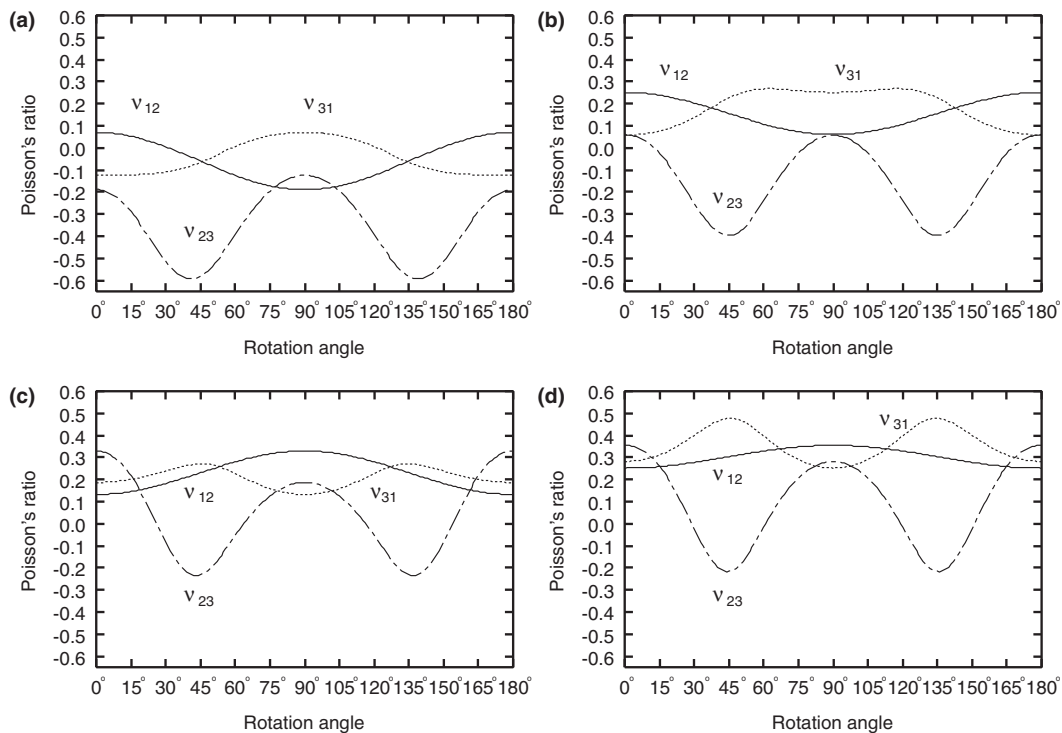


Fig. 6 Variation in Poisson's ratios of α -cristobalite for a uniaxial loading as the crystals are rotated about the a axis from the b axis. (a) 0 GPa, (b) 2 GPa, (c) 5 GPa, (d) 10 GPa.

typical model of auxetic crystals. However, the BKS model is not so successful in describing the compressive behavior and the high-pressure elasticity of cristobalite, compared with the DFT calculations. We have applied the elastic constants derived from our calculations to study the isotropic average and directional dependence of Poisson's ratios in the crystal. It is predicted that cristobalite exhibits a negative Poisson's ratio only in the pressure range of ca. ~ 2 GPa, while the Poisson's ratio shows a strong anisotropic behavior up to 10 GPa. We present that the compressive behavior in the cristobalite structure is dominated by the cooperative rotations of corner-linked SiO_4 tetrahedra at molecular level. To this end, our simulations give satisfactory results and enables us to analyze the anomalous behavior of the elastic properties in this system, while the effect of the internal degrees of freedom within the system is taken into account under hydrostatic pressure.

Acknowledgements

H. K. would like to thank Hideo Kaburaki for his support during the research.

REFERENCES

- 1) A. Yeganeh-Haeri, D. J. Weidner and J. B. Parise: *Science* **257** (1992) 650–652.
- 2) N. R. Keskar and J. R. Chelikowsky: *Nature (London)* **358** (1992) 222–224.
- 3) H. Kimizuka, H. Kaburaki and Y. Kogure: *Phys. Rev. Lett.* **84** (2000) 5548–5551.
- 4) A. Alderson and K. E. Evans: *Phys. Rev. Lett.* **89** (2002) 225503 (4 pages).
- 5) R. S. Lakes: *Science* **235** (1987) 1038–1040.
- 6) K. E. Evans, M. A. Nkansah, I. J. Hutchinson and S. C. Rogers: *Nature (London)* **353** (1991) 124.
- 7) K. E. Evans and A. Alderson: *Adv. Mater.* **12** (2000) 617–628.
- 8) B. W. H. van Beest, G. J. Kramer and R. A. van Santen: *Phys. Rev. Lett.* **64** (1990) 1955–1958.
- 9) G. Kresse and J. Furthmüller: *Phys. Rev. B* **54** (1996) 11169–11186.
- 10) P. E. Blöchl: *Phys. Rev. B* **50** (1994) 17953–17979.
- 11) G. Kresse and D. Joubert: *Phys. Rev. B* **59** (1999) 1758–1775.
- 12) D. M. Ceperley and B. J. Alder: *Phys. Rev. Lett.* **45** (1980) 566–569.
- 13) J. P. Perdew and A. Zunger: *Phys. Rev. B* **23** (1981) 5048–5079.
- 14) J. J. Pluth, J. V. Smith and J. Faber, Jr.: *J. Appl. Phys.* **57** (1985) 1045–1049.
- 15) H. J. Monkhorst and J. D. Pack: *Phys. Rev. B* **13** (1976) 5188–5192.
- 16) P. E. Blöchl, O. Jepsen and O. K. Andersen: *Phys. Rev. B* **49** (1994) 16223–16233.
- 17) S. Nosé: *Mol. Phys.* **52** (1984) 255–268.
- 18) W. G. Hoover: *Phys. Rev. A* **31** (1985) 1695–1697.
- 19) M. Parrinello and A. Rahman: *J. Appl. Phys.* **52** (1981) 7182–7190.
- 20) J. R. Ray, M. C. Moody and A. Rahman: *Phys. Rev. B* **32** (1985) 733–735.
- 21) D. C. Palmer and L. W. Finger: *Am. Miner.* **79** (1994) 1–8.
- 22) R. T. Downs and D. C. Palmer: *Am. Miner.* **79** (1994) 9–14.
- 23) R. J. Hemley, C. T. Prewitt and K. J. Kingma: *Rev. Mineral.* **29** (1994) 41–81.
- 24) L. Levien and C. T. Prewitt: *Am. Miner.* **66** (1981) 324–333.
- 25) N. L. Ross, J.-F. Shu, R. M. Hazen and T. Gasparik: *Am. Miner.* **75** (1990) 739–747.
- 26) S. Tsuneyuki, M. Tsukada, H. Aoki and Y. Matsui: *Phys. Rev. Lett.* **61** (1988) 869–872.
- 27) H. Kimizuka and H. Kaburaki: *Phys. Status Solidi B* **242** (2005) 607–620.
- 28) R. F. Almgren: *J. Elasticity* **15** (1985) 427–430.
- 29) A. G. Kolpakov: *Prikl. Matem. Mekhan.* **49** (1985) 969–977 [*J. Appl. Math. Mech.* **49** (1985) 739–745].
- 30) L. J. Gibson and M. F. Ashby: *Cellular Solids: Structure & Properties*, (Pergamon, Oxford, 1988).